Research Square

Preprints are preliminary reports that have not undergone peer review.
They should not be considered conclusive, used to inform clinical practice,
or referenced by the media as validated information.

Optimization and Construction of the Thickness and Strength of the Sealing Wall in the Connecting Roadway

Dong Zhang
National Institute of Clean and Low-Carbon Energy
Yang Dong
National Institute of Clean and Low-Carbon Energy
Xia Wang
National Institute of Clean and Low-Carbon Energy
Siyu Gong
2181283734@qq.com
National Institute of Clean and Low-Carbon Energy
Dehai Lin
National Institute of Clean and Low-Carbon Energy
Jinzhu Huang
Jiangxi University of Technology
Rui Wu
Jiangxi University of Technology

Article

Keywords: Connecting roadway, Flexible formwork sealing wall, Vehicle-mounted pumping, Numerical simulation, Synergistic control

Posted Date: July 3rd, 2026

DOI: https://doi.org/10.21203/rs.3.rs-10045155/v1

License: This work is licensed under a Creative Commons Attribution 4.0 International License.
Read Full License

Additional Declarations: No competing interests reported.

Version of Record: A version of this preprint was published at Scientific Reports on October 9th, 2026. See the published version at https://doi.org/10.1038/s41598-026-70505-6.

Optimization and Construction of the Thickness and Strength of the Sealing Wall in the Connecting Roadway

Dong Zhang,[1] Yang Dong,[1] Xia Wang,[1] Siyu Gong,[1,*] Dehai Lin,[1] Jinzhu Huang,[2] and Rui Wu,[2]

[1]National Institute of Clean and Low-Carbon Energy (China), Beijing, 102211, China
[2]Jiangxi University of Science and Technology, Ganzhou, Jiangxi, 341000, China

Correspondence should be addressed to Siyu Gong; 2181283734@qq.com

Abstract

Addressing the engineering challenges of instability and air leakage in sealing walls within connecting roadways under the influence of intensive mining-induced dynamic pressure in shallow-buried mines, this study employs FLAC3D numerical simulation to systematically investigate the effects of sealing wall thickness (0.8m–1.4m) and concrete strength grades (C10–C30) on the surrounding rock mass displacement, wall stress, and multidimensional strain evolution. The results indicate that the effect of sealing wall thickness on roof subsidence control exhibits a significant "diminishing marginal effect," with 1.0m identified as the efficiency inflection point for displacement control, which ensures that the critical load-bearing wall crosses the dangerous critical state into a safe bearing zone. At a thickness of 1.0m, the concrete strength grade shows a non-linear exponential decay negative correlation with the maximum principal strain and maximum shear strain within the wall. The C25 strength grade is identified as the optimal strength grade within the 'rigid-flexible synergistic equilibrium zone, where the sealing wall effectively suppresses penetrating shear failure while maximizing the pressure-relief and energy-absorption characteristics inherent to the flexible formwork system. Based on these optimal parameters, a set of rapid construction technologies for flexible formwork sealing walls based on a vehicle-mounted pumping system is proposed and applied, achieving full-section precise roof contact and mechanized efficient forming of the sealing wall. The research results provide a complete set of processes and theoretical basis for the efficient and reliable sealing of roadways under intensive shallow dynamic pressure.

Keywords: Connecting roadway; Flexible formwork sealing wall; Vehicle-mounted pumping; Numerical simulation; Synergistic control

1. Introduction

The sealing wall in the connecting roadway of a coal mine serves as a core safety barrier for isolating the goaf, blocking air leakage paths, preventing spontaneous combustion-induced fires, and resisting the shock waves of gas explosions. In recent years, with the widespread application of high-mining-height technology in shallow-buried coal seams, intensive mining-induced dynamic pressure and dramatic overlying strata movement have exacerbated the deformation of the surrounding rock in roadways. A novel composite sealing wall constructed using flexible formwork can effectively adapt to significant rock deformation, thereby significantly enhancing the overall stability of the sealing system. However, in the engineering design of these novel sealing walls, a critical scientific challenge remains: how to scientifically and quantitatively determine the "rational thickness" of the wall and the "rational strength" of the materials, so as to avoid either structural failure due to insufficient design thickness or excessive cost caused by over-designing.

Scholars both domestically and internationally have conducted extensive and fruitful research on the stress characteristics, thickness design, and parameter optimization of mine sealing walls. Regarding basic parameter determination and structural optimization, Lu et al. (2014) explored rational parameters for sealing walls in fully mechanized top-coal caving connecting roadways; Wei (2009) performed stability analysis on new types of permanent mine seals; Zheng (2002) systematically studied design methods for large-scale goaf sealing walls; and Huang et al. (2014) performed stress calculation and optimization analysis on filling sealing walls in underground goaf. Regarding resistance to dynamic impact and gas explosion loads, the ultimate bearing capacity of sealing walls is a focal point of research. Jing et al. (2017) analyzed the anti-explosion impact safety of sealing walls based on ANSYS numerical simulation; Zhang (2021) and Cheng and Zhang (2021) conducted in-depth studies on the stress state, stability, and damage assessment methods of sealing walls under explosion loads; and Sun (2021), Liu (2019), and Li et al. (2008) explored the mechanism of impact-resistant sealing walls in large-area roof-hanging goaf and the effects of mine earthquake shock waves from perspectives including design methods, numerical simulation, and experimental analysis. In terms of English-language literature, Hu et al. (2025) revealed gas explosion laws and established a method for determining the safe thickness of auxiliary roadway retaining walls; and Jianwei et al. (2020) conducted an in-depth study on the stability characteristics of sealing walls in underground coal mines under the coupling effect of explosion loads and ground pressure. Regarding classic theoretical derivation and reliability assessment of waterproof sealing walls, the academic community has established a solid mechanical foundation. Yan (1965), Chen (1966), and Yi (1976) conducted classic theoretical discussions on the rational calculation of waterproof sealing walls in their early work, laying the foundation for mechanical models of sealing walls; Du et al. (2025), Zhang (2015), and Yang (2015) further improved the stability evaluation and reliability research for waterproof sealing walls and water storage chambers in connecting

roadways; Douglas (2006) reviewed the development history of thickness design for underground mine grouting waterproof retaining walls; Harteis and Dolina (2006) discussed design and safety considerations for underground mine water and mud retaining walls; and Yuan et al. (2022) studied the seepage failure characteristics between retaining walls and surrounding rock in deep underground mines through experiments. Regarding mine pressure manifestation, filling material failure characteristics, and flexible formwork numerical simulation, Mu (2007) discussed the application of mine pressure in goaf sealing walls; Li et al. (2020) revealed the deformation and failure characteristics and reinforcement measures of sealing walls affected by mining in coal-pillar working faces; Li (2015) performed numerical simulations of fly ash solidification filling characteristic parameters; and Guo et al. (2005) conducted numerical simulation research on full-scale underground retaining walls and adjacent rock masses under fully coupled thermal-hydro-mechanical conditions. Regarding the mechanical mechanism of the flexible formwork process, Xie et al. (2020) analyzed the stability of flexible concrete formwork in the overall load-bearing structure of surrounding rock in roadway-side packing; Wang and Guo (2025) studied the deformation and failure mechanisms of flexible formwork walls in ultra-long island working faces; and Cao et al. (2025) conducted a comprehensive data analysis on the application of flexible formwork technology in steeply dipping coal seams.

In summary, existing research has achieved fruitful results in the calculation of anti-explosion thickness for sealing walls, classic mechanical derivation, and the failure characteristics of flexible formwork materials. However, most existing literature focuses on ultimate bearing capacity calculation under single working conditions or solely investigates the construction technology of flexible formwork walls. There is a lack of systematic research that treats "sealing wall thickness" and "sealing wall material strength" as dual variables to study their synergistic matching laws under the coupling effects of complex intensive dynamic pressure and lateral loads.

Based on this, this paper takes a coal mine connecting roadway as the engineering background and combines classic mechanical derivation with FLAC3D three-dimensional numerical simulation to conduct a quantitative study on the "rational strength" and "rational thickness" of flexible formwork sealing walls. By analyzing the stress distribution, overlying strata displacement, and plastic zone evolution of sealing walls under different strength-to-thickness ratios, this study proposes optimization design criteria that prioritize both safety and economy, aiming to provide a reliable theoretical basis and parameter guidance for the construction of novel sealing systems in shallow mine environments subjected to intensive dynamic pressure.

2. Engineering Background

2.1 General Overview of the Mine

This study is based on the Sandaogou Coal Mine of China Energy Investment Corporation, with the target horizon being the 5-2 coal seam of the Middle-Lower Jurassic. The coal seam is characterized by a gentle attitude, with an inclination angle maintained between 1° and 3°. Faults within the mine field are rarely developed, and the geological structure is extremely simple. The average thickness of the 5-2 coal seam reaches approximately 6.5m. It possesses significant characteristics such as low sulfur, low phosphorus, and low ash content, classifying it as high-quality power coal. Regarding the mechanical properties of the surrounding rock, the spatial environment of the sealing wall is significantly controlled by the lithology of the roof and floor. The thickness of the immediate roof of the working face ranges from 4.5m to 6.6m; its lithology is primarily composed of gray massive mudstone, exhibiting obvious weak and soft mechanical properties with limited compressive strength. The main roof consists of thicker muddy siltstone or medium-grained feldspar sandstone, with a thickness range of 13.3m to 14.3m, providing the primary macro-scale load-bearing skeleton for the roadway. The immediate floor of the roadway is mainly composed of dark gray siltstone or mudstone, showing typical sedimentary rock sequence characteristics. Overall, the large-scale mining of the thick coal seam, superimposed on the inherent defects of the weak immediate roof, makes the connecting roadway highly susceptible to significant squeezing and deformation under the intensive mining environment. These harsh and unstable surrounding rock conditions impose rigorous requirements on the overall compressive performance and geometric thickness of the sealing system, which also form the critical engineering mechanical boundaries for the subsequent derivation of the sealing wall's rational strength and thickness optimization in this paper.

2.2 Overview of the Working Face and Roadway Layout

The spatial layout of this study area is centered on the 85220 fully mechanized mining working face and its adjacent 85222 working face. As shown in Figure 1, the 85220 Haulage roadway and the 85222 Return roadway are arranged in parallel and in close proximity, isolated by a sectional coal pillar. To meet the requirements for early ventilation and system connectivity, a transverse connecting roadway was excavated within the coal pillar. With the continuous advance of the working face, to effectively isolate the goaf, block air leakage paths, and prevent the overflow of toxic and harmful gases such as methane, it is essential to construct a secure fire prevention and extinguishing sealing system within the connecting roadway.

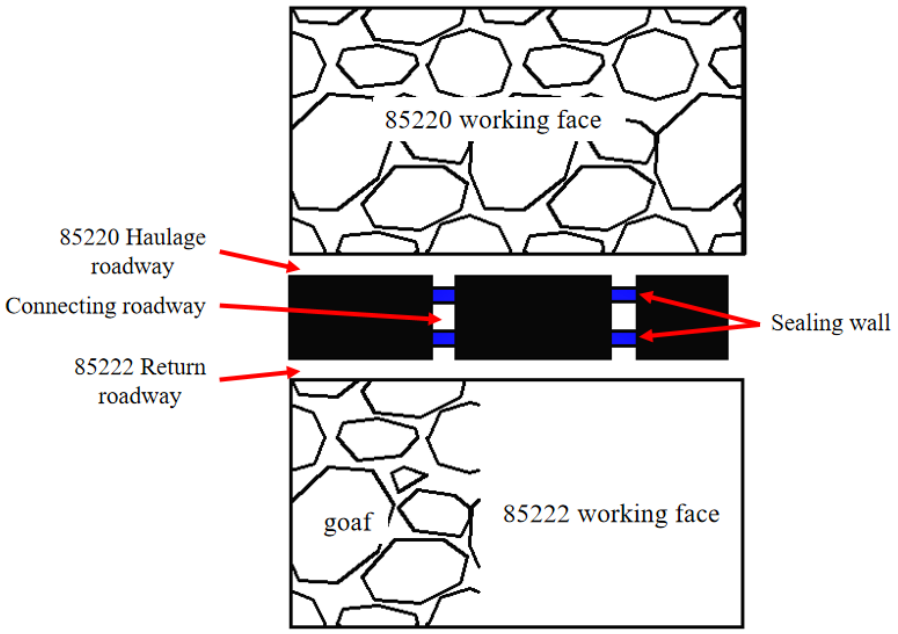


Figure 1. Layout plan of the 85220 and 85222 adjacent working faces and the sealing walls in the connecting roadway

Based on previous engineering practices and the requirements for surrounding rock control, this area has abandoned the traditional single-thick solid wall in favor of a "double-sealing wall" spatial layout scheme based on synergistic load-bearing. Specifically, within the connecting roadway linking the two roadways, a flexible formwork concrete sealing wall (indicated in blue in the figure) is constructed at a distance of 5m from the entrance of the 85220 Haulage roadway and 5m from the entrance of the 85222 Return roadway, respectively. The two walls form a series-connected dual-defense system in space.

This specific spatial layout imposes extremely high optimization requirements on the geometric dimensions and mechanical parameters of the sealing walls. On one hand, with the mining of the working faces on both sides, the connecting roadway and the intermediate coal pillar will be subjected to extremely intense superimposed advanced abutment pressure. As isolation structures, the sealing walls must possess sufficient structural strength to resist the severe squeezing and large deformation of the surrounding rock. On the other hand, in this dual-wall system, the thickness and material strength of a single wall directly determine the overall stiffness and pressure-relief/energy-absorption characteristics of the system. If the wall is designed to be too thin or the strength is too low, it is highly susceptible to crushing instability and air-tightness failure under intensive mining. Conversely, blindly increasing the wall thickness or using materials with excessively high strength grades not only leads to surging construction costs and prolonged construction periods, but may also cause the system to lose its deformation coordination ability, thereby triggering more severe local stress concentration and brittle fracture. Therefore, based on this dual-wall layout, scientifically exploring the "rational thickness" and "rational strength" of the

single sealing wall is the key prerequisite for ensuring the long-term stability and economic efficiency of the sealing system in this area.

3. Numerical Calculation Model for Sealing Wall Thickness and Strength

To truly restore the complex dynamic pressure evolution path induced by the sequential mining of dual working faces in the shallow-buried geological environment, as well as the disturbance effect of this path on the novel flexible formwork sealing system in the connecting roadway, this paper builds a full-scale three-dimensional elastic-plastic numerical calculation model based on the finite difference software FLAC3D 7.00 to conduct quantitative optimization of the rational thickness and strength of the sealing walls.

3.1 Three-Dimensional Numerical Calculation Model and Boundary Conditions

Combined with the actual geological drilling data of the mine, an overall three-dimensional numerical model including the coal seam, roof and floor strata, and the roadway group of the working face was established. The overall grid division of the model is shown in Figure 2.

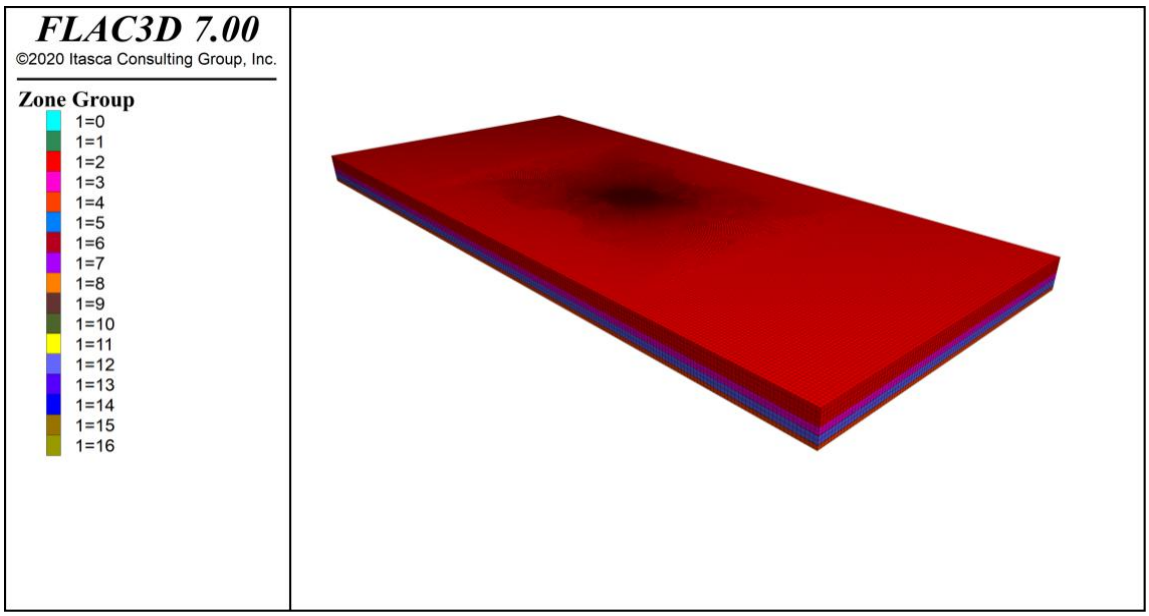


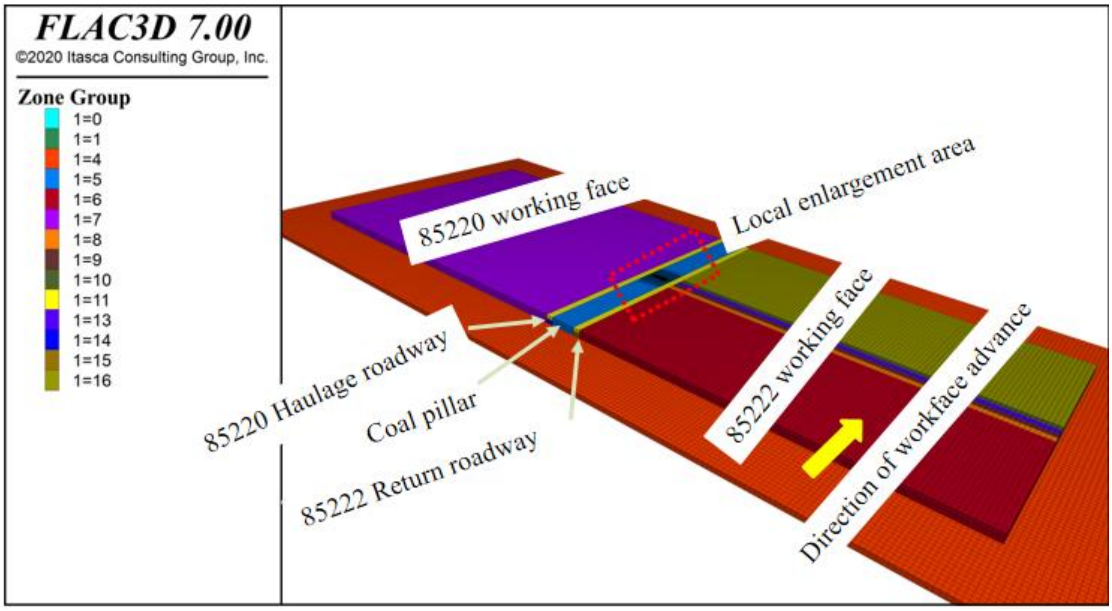
Figure 2 Overall mesh of the numerical model.

Considering that the engineering background involves a typical shallow-buried mine, the upper boundary of the model is subjected to an equivalent vertical uniform load based on the actual burial depth to simulate the self-weight stress of the overlying strata. The bottom boundary of the model is constrained in the vertical direction

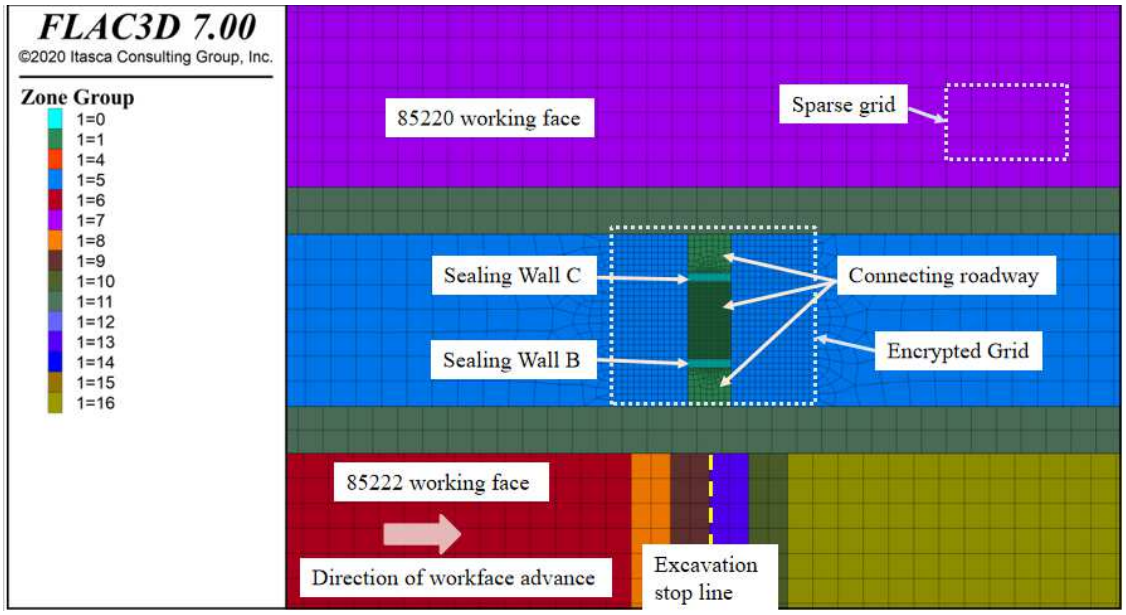
(Z-direction) by fixing displacements, and horizontal displacement constraints are applied to the lateral boundaries of the model (fixing X-direction and Y-direction displacements, respectively). The horizontal stress coefficient is set according to the results of shallow rock mechanics tests to accurately simulate the initial in-situ stress field in this shallow-buried region.

3.2 Spatial Layout and Grid Topology Optimization of the Working Face

To eliminate boundary effects and precisely capture the localized strain concentration characteristics of the sealing walls, a topology optimization strategy of "global sparse, local progressive refinement" is adopted for the spatial arrangement and grid discretization. The spatial layout of each working face, roadway, and sealing wall is shown in Figure 3.



(a) Layout of working faces and roadways



(b) Grid discretization of the novel sealing wall (local enlargement area of Figure 3a).

Figure 3. Spatial layout of the working faces, roadways, and sealing walls.

As shown in Figure 3a, the main body of the model includes the 85220 working face and the 85222 working face, with a sectional coal pillar left between the two. The 85220 Haulage roadway and the 85222 Return roadway are used for ventilation and transportation, and a connecting roadway is excavated between the two roadways. To reduce computational resource consumption, large-size sparse grids are adopted for the peripheral rock mass far from the mining disturbance zone (e.g., the outside of the working face). In contrast, in the connecting roadway and the sealing wall areas (as shown in the local enlargement of Figure 3b), because they are the core research objects of deformation and failure, high-density encrypted grids are applied. Sealing Wall B and Sealing Wall C are arranged in parallel in the connecting roadway. This refinement of the mesh provides the geometric foundation for capturing the minute principal strain and shear strain within the filling body during subsequent analysis.

3.3 Selection of Physical and Mechanical Parameters and Constitutive Models

The loading and failure processes of the coal mass and various rock strata (siltstone, mudstone, muddy siltstone, etc.) in the model all conform to the Mohr-Coulomb elastic-plastic yield criterion. Due to their specific pressure-relief characteristics, the flexible formwork paste filling materials used for the sealing walls are assigned specialized mechanical parameters as independent solid elements. Combined with the results of laboratory rock mechanics tests and filling material ratio tests, the main physical and mechanical parameters of the coal, rock mass, and sealing wall (taking a specific reference strength as an example) in the model are shown in Table 1.

Table 1 Physical and Mechanical Parameters of Coal, Rock, and Sealing Walls

Lithology	Tensile Strength R_t/ MPa	Shear Modulus S/GPa	Bulk Modulus B/GPa	Cohesion C/MPa	Friction Angleφ/°	Density γ/(kg/m^3)
5^{-2}Coal	0.8	4.6	2.8	1.5	29	1300
Siltstone	8.5	8.13	10.83	9.2	40	2570
Mudstone	4	5.0	8.2	8.5	35	2350
Argillaceous Siltstone	5	5.8	9.6	9.8	37	2580
Sealing Wall C30	2.5	30	12.5	3.0	35	2400
Sealing Wall C25	1.78	25.6	11.2	2.78	33	2400
Sealing Wall C20	1.1	20.2	10.2	2.54	32	2400
Sealing Wall C10	0.84	19.7	8.7	1.77	30	2400

3.4 Dynamic Excavation Sequence and Monitoring Section Setup

The sequential mining order of the dual working faces is the fundamental factor determining the stress state of the sealing walls in the connecting roadway. To realistically reproduce the spatio-temporal evolution process in the underground mine, the numerical calculation strictly follows the dynamic excavation sequence and section monitoring logic shown in Figure 4.

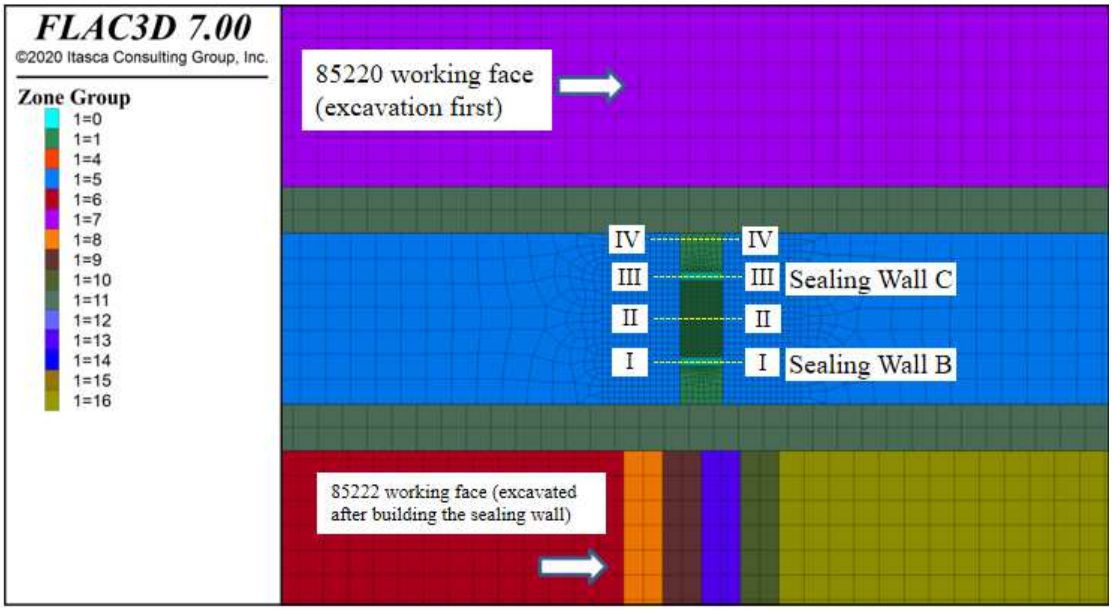


Figure 4. Layout of the monitoring sections (I-I to IV-IV) for the sealing wall system.

In response to the asymmetric excavation sequence of the dual working faces, the numerical simulation first computes the initial in-situ stress equilibrium, followed by the preferential excavation of the 85220 working face (first-excavation zone) to simulate the initial caving of the goaf roof and the subsequent stress redistribution. Subsequently, Sealing Wall B and Sealing Wall C are constructed within the connecting roadway. Finally, the 85222 working face (later-excavation zone) is advanced. This spatio-temporal evolution path—involving initial single-sided mining, subsequent wall construction, and final dual-sided mining—results in Sealing Wall C bearing a more severe asymmetric abutment pressure from the goaf side, whereas Sealing Wall B primarily sustains the advance dynamic pressure from the working face, thereby forming an asymmetric stress boundary.

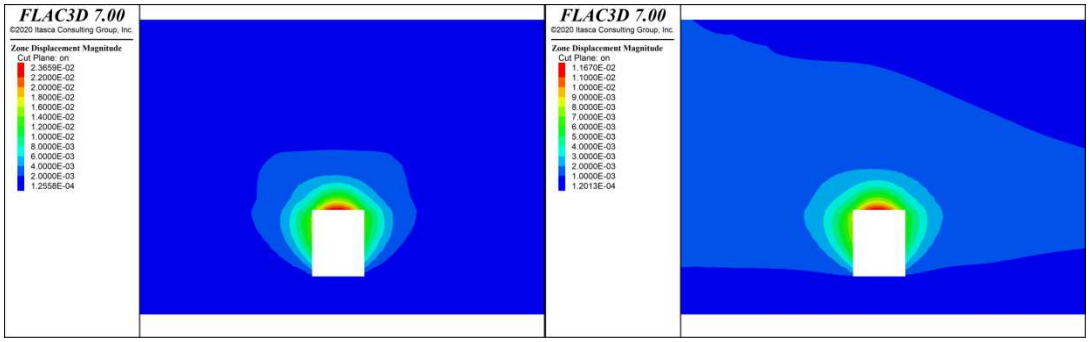
To comprehensively capture the mechanical response of the sealing system under the aforementioned excavation path, four key cross-sections were set along the axis of the connecting roadway from bottom to top (as indicated by the dashed lines in Figure 4) for multidimensional monitoring. Specifically, the I-I section traverses the core load-bearing zone of Sealing Wall B; the II-II section traverses the connecting roadway roof between the two walls, primarily used to monitor the displacement and subsidence laws of the surrounding rock in the unsupported middle area; the III-III section traverses the core load-bearing zone of Sealing Wall C and serves as a high-stress control zone for the entire anti-air-leakage system; and the IV-IV section is positioned on the outer side of Sealing Wall C, near the edge of the 85220 goaf, specifically designed to monitor the ultimate displacement of the surrounding rock subjected to severe asymmetric loading.

4. Study on Sealing Wall Thickness

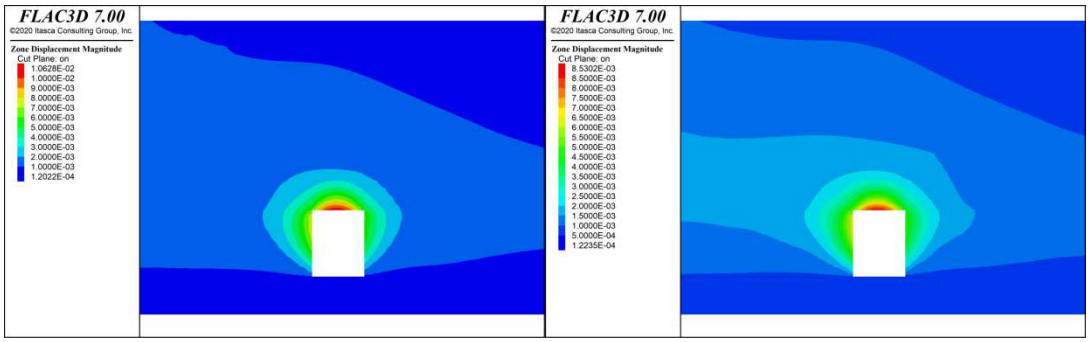
4.1 Influence of Thickness on Surrounding Rock Displacement Characteristics

(1) Analysis of the II-II Section

Based on the aforementioned analysis of displacement characteristics, it is evident that the thickness of the sealing wall exerts a significant control effect on the deformation of the surrounding rock in the connecting roadway. However, according to the principle of action and reaction in rock mechanics, the cost of restricting the deformation of surrounding rock is inevitably that the sealing wall itself must sustain higher compressive stress. Therefore, to further investigate the impact of sealing wall thickness on its own bearing capacity, the sealing wall at the I-I section was extracted for analysis. With the concrete strength grade set at C30, the vertical stress distribution within the wall was compared and analyzed for sealing wall thicknesses of 0.8m, 1.0m, 1.2m, and 1.4m, respectively. The stress cloud diagrams are shown in Figure 5.



(a)0.8m (b)1.0m



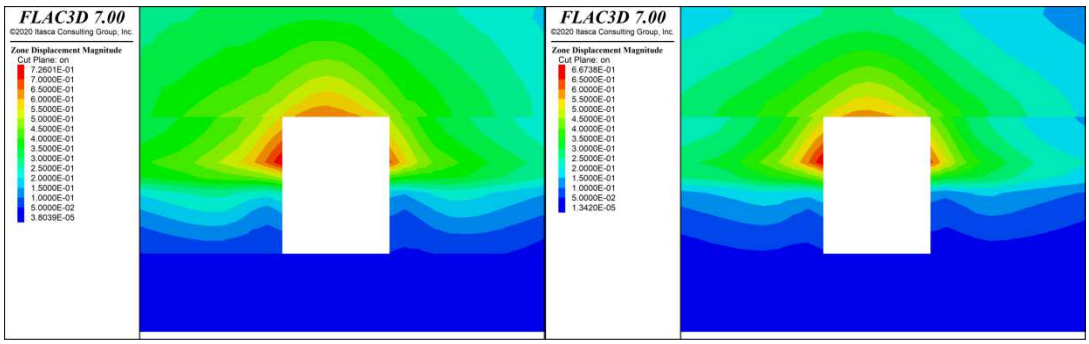
(c)1.2m (d)1.4m

Figure 5. Cloud diagram of surrounding rock displacement in the connecting roadway.

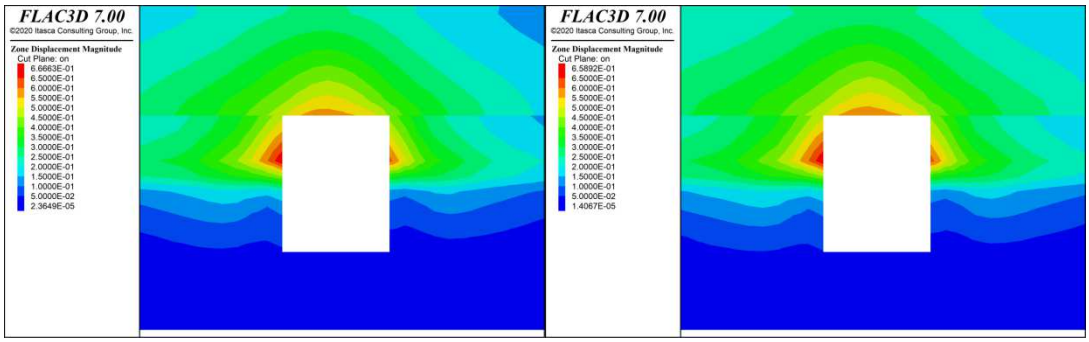
As shown in the evolution patterns of the displacement cloud diagrams in Figure 5, under the combined effects of in-situ stress and mining-induced stress, the deformation of the connecting roadway is primarily concentrated in the roof area. The displacement contour lines typically exhibit a "semi-elliptical" expansion characteristic, centered at the roadway roof and extending into the deep surrounding rock. With the increase in sealing wall thickness, the maximum displacement of the surrounding rock shows a clear decreasing trend. When the sealing wall thickness is 0.8m (as shown in Figure 5a), the maximum displacement of the overlying strata reaches approximately 23.6mm. When the thickness increases to 1.0m (as shown in Figure 5b), the displacement characteristics of the surrounding rock are significantly improved; the maximum roof displacement drops sharply to approximately 11.6mm. As the sealing wall thickness further increases to 1.2m (Figure 5c) and 1.4m (Figure 5d), the maximum roof displacement decreases to approximately 10.6mm and 8.5mm, respectively.

(2) Analysis of the IV-IV Section

To evaluate the impact of sealing wall thickness on the displacement of the surrounding rock in the connecting roadway, the IV-IV monitoring section was further extracted for comparative analysis. Assuming a concrete strength of C30 for the sealing wall, the displacement cloud diagrams of the surrounding rock corresponding to different sealing wall thicknesses (0.8m, 1.0m, 1.2m, and 1.4m) are shown in Figure 6.



(a)0.8m (b)1.0m



(c)1.2m (d)1.4m

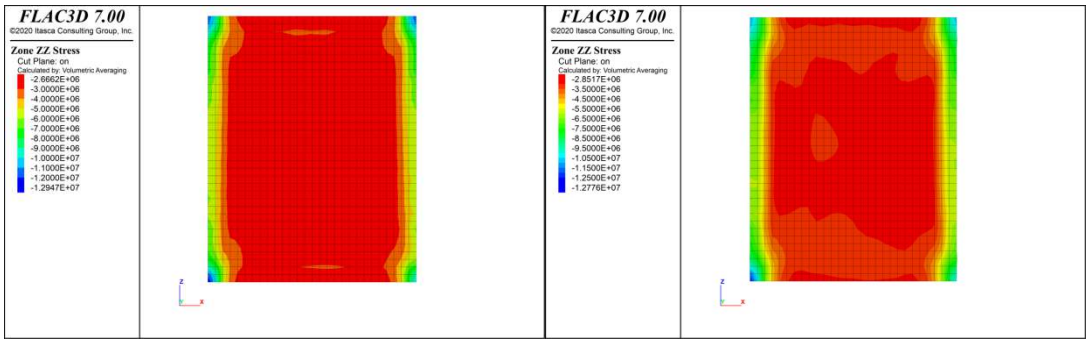
Figure 6. Cloud diagram of surrounding rock displacement in the connecting roadway.

It can be observed from Figure 6 that the surrounding rock deformation at the IV-IV section exhibits a distinct failure pattern characterized by "stress concentration at the shoulders, extending into the deep rock mass." High displacement concentration zones (red areas) appear at both shoulders of the roadway roof. As the sealing wall thickness increases, the maximum displacement of the surrounding rock shows a clear decreasing trend. When the sealing wall thickness is 0.8m (as shown in Figure 6a), the maximum displacement of the surrounding rock surges to approximately 726.0mm. When the thickness increases to 1.0m (as shown in Figure 6b), the maximum displacement at the roof and shoulders drops significantly to approximately 667.4mm. As the sealing wall thickness further increases to 1.2m (as shown in Figure 6c) and 1.4m (as shown in Figure 6d), the maximum displacement values decrease to approximately 666.6mm and 658.9mm, respectively.

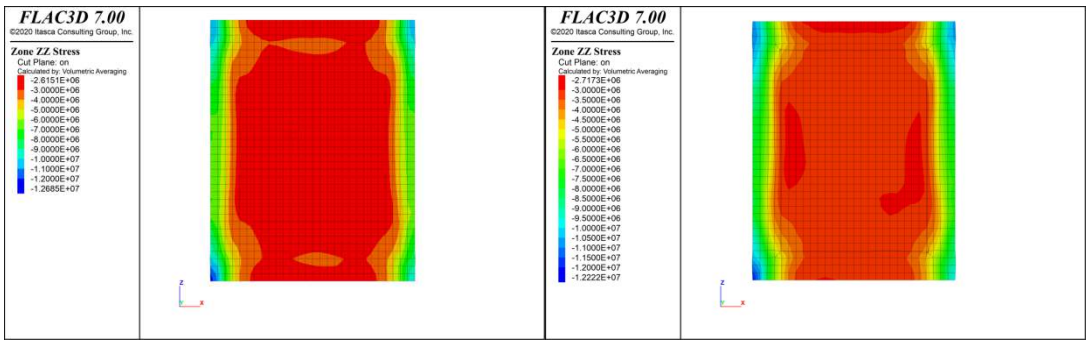
4.2 Influence of Thickness on Stress Distribution Characteristics of the Sealing Wall

(1) Analysis of the I-I Section

To investigate the impact of sealing wall thickness on its own bearing capacity, the sealing wall at the I-I section was extracted for analysis. Under the condition that the concrete strength grade of the sealing wall is C30, the vertical stress distribution patterns within the wall were compared and analyzed for thicknesses of 0.8m, 1.0m, 1.2m, and 1.4m. The corresponding stress cloud diagrams are shown in Figure 7.



(a)0.8m (b)1.2m



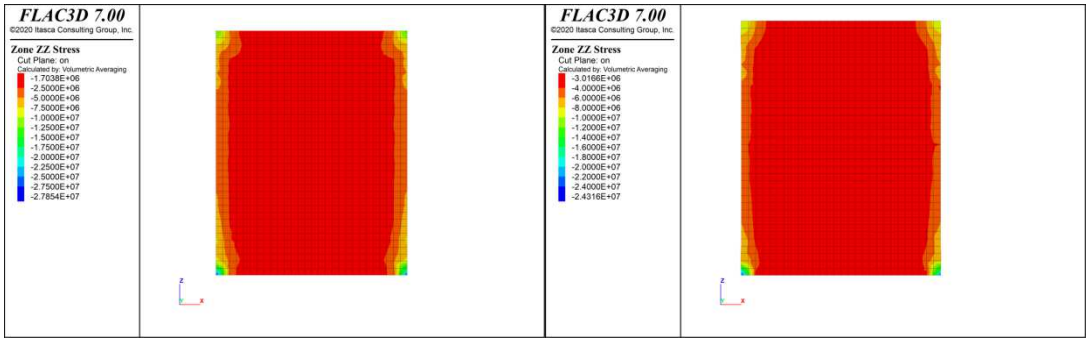
(c)1.2m (d)1.4m

Figure 7. Stress cloud diagram of the sealing walls.

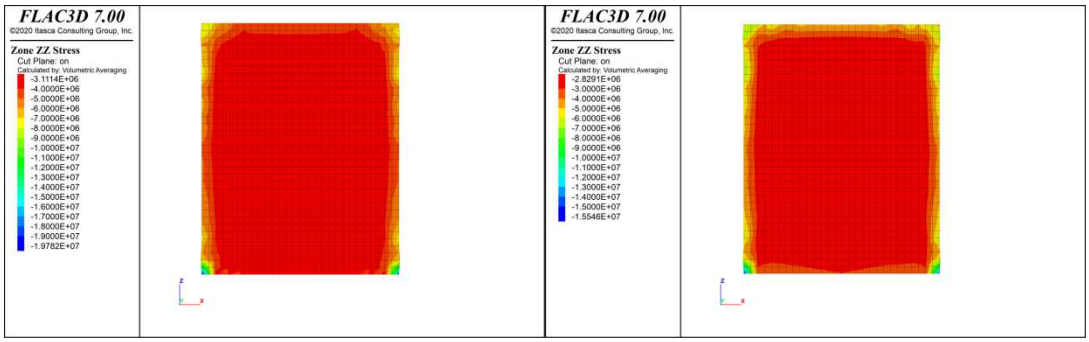
As observed from the overall stress distribution patterns in Figure 7, the internal stress of the sealing wall exhibits a distinct "core-ring" distribution characteristic. As the thickness increases, the peak stress shows a continuous decreasing trend. When the sealing wall thickness is 0.8m (as shown in Figure 7a), the peak maximum compressive stress reaches 12.95 MPa. When the thickness increases to 1.0m (as shown in Figure 7b), the peak maximum compressive stress drops to 12.78 MPa. As the thickness is further increased to 1.2m (Figure 7c) and 1.4m (Figure 7d), the peak maximum compressive stress continues to decrease, falling to 12.69 MPa and 12.22 MPa, respectively.

(2) Analysis of the III-III Section

To further evaluate the impact of sealing wall thickness on its bearing capacity, the III-III section was extracted for comparative analysis. Compared with Sealing Wall B, Sealing Wall C exhibits a significantly higher overall stress level due to the more intense mining-induced advanced abutment pressure and asymmetric loading. Under the condition that the concrete strength grade is C30, the vertical stress distribution within Sealing Wall C for different thicknesses (0.8m, 1.0m, 1.2m, and 1.4m) is shown in Figure 8.



(a)0.8m (b)1.0m



(c)1.2m (d)1.4m

Figure 8. Stress cloud diagram of Sealing Wall C.

As shown in Figure 8, the internal stress of Sealing Wall C similarly exhibits a "core-ring" distribution pattern. As the thickness increases, the peak stress shows a continuous decreasing trend. When the sealing wall thickness is 0.8m (as shown in Figure 8a), the peak maximum compressive stress reaches as high as 27.85 MPa. When the thickness increases to 1.0m (as shown in Figure 8b), the peak maximum compressive stress drops significantly to 24.32 MPa. As the thickness is further increased to 1.2m (Figure 8c) and 1.4m (Figure 8d), the peak maximum compressive stress continues to decrease, falling to 19.78 MPa and 15.55 MPa, respectively.

4.3 Comparative Analysis and Determination of Rational Thickness

(1) Displacement Comparative Analysis

To quantitatively reveal the control laws between sealing wall thickness and roadway roof deformation more intuitively, the maximum roof displacement data extracted from the aforementioned numerical simulations were fitted to plot the relationship curves between the thicknesses of Sealing Wall B and Sealing Wall C and the maximum roof displacement, as shown in Figures 9 and 10.

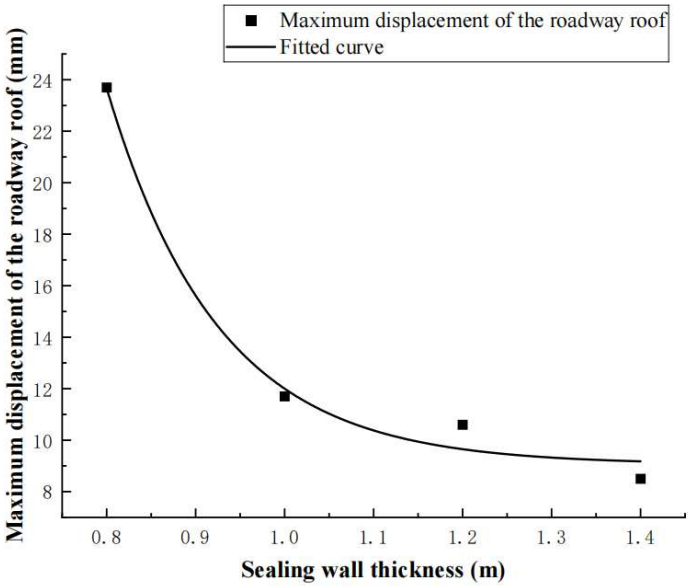


Figure 9. Relationship between the thickness of Sealing Wall B and the roof displacement of the roadway.

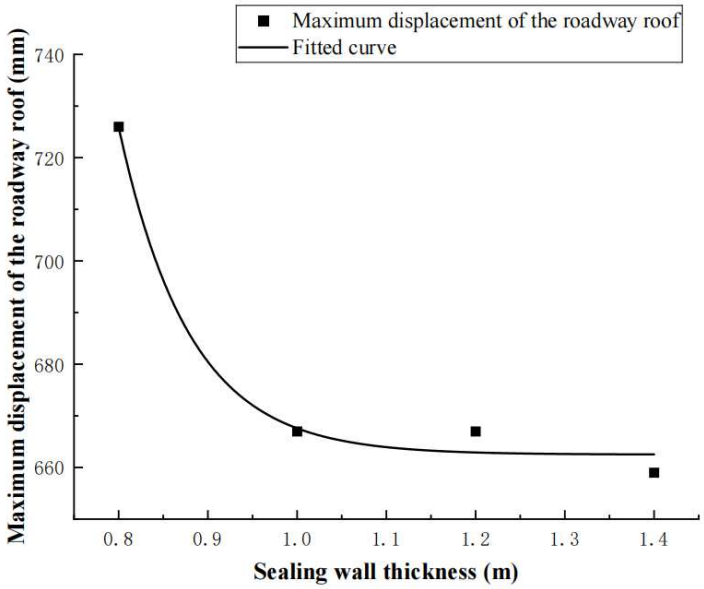


Figure 10. Relationship between the thickness of Sealing Wall C and the roof displacement of the roadway.

As can be observed from the overall morphology of the two sets of fitted curves, both Sealing Wall B and Sealing Wall C exhibit a highly consistent non-linear negative correlation between thickness and roof subsidence, with the curves displaying a typical "diminishing marginal effect." When the sealing wall thickness x is between 0.8m and 1.0m, the maximum roof displacement of the roadway decreases sharply

with increasing thickness. Specifically, the roof displacement for Sealing Wall B drops abruptly from 23.6mm to 11.6mm, a reduction of over 50%, while the roof displacement for Sealing Wall C also falls steeply from 726mm to approximately 667mm. When the thickness x ≥ 1.0m, the maximum roof displacement exhibits an obvious "inflection point" and subsequently tends to flatten, showing a significant law of diminishing marginal utility and gradually approaching a non-zero ultimate residual displacement as the thickness continues to increase. In the thickness range of 1.0m to 1.4m, although the roof displacement continues to decrease slightly, the slope is minimal; despite a 40% increase in wall thickness, the improvement in roof displacement is merely in the single-digit millimeter range. This indicates that once the thickness exceeds 1.0m, further increasing the sealing wall thickness has a negligible impact on surrounding rock displacement.

Based on the variation of maximum roof displacement with sealing wall thickness, the reasonable hypothetical model for fitting is the Exponential decay function model, expressed as:

$$y = y_0 + A \cdot e^{-k \cdot x} \quad (1)$$

where y0、A、k are undetermined parameters related to the displacement attenuation characteristics of the roadway roof; y is the maximum roof displacement of the roadway (mm); and x is the sealing wall thickness (m).

According to the extracted numerical data of sealing wall thickness and maximum roof displacement, the fitted curve is:

$$y = 9.06 + 8897.08 \cdot e^{0.13 \cdot x} \quad (2)$$

Through the comparative analysis of the displacement relationships above, it can be concluded from the perspectives of surrounding rock deformation control and economic feasibility that a sealing wall thickness of 1.0m is a key "inflection point" for controlling roadway displacement under these geological conditions, serving as the critical point for the rational thickness.

(2) Stress Comparative Analysis

Beyond the control of surrounding rock deformation, the load-bearing safety of the sealing wall itself is another core indicator of parameter design. The maximum vertical compressive stress data within Sealing Wall B and Sealing Wall C were extracted from the numerical simulations to plot the relationship curves with wall thickness, as shown in Figures 9 and 10.

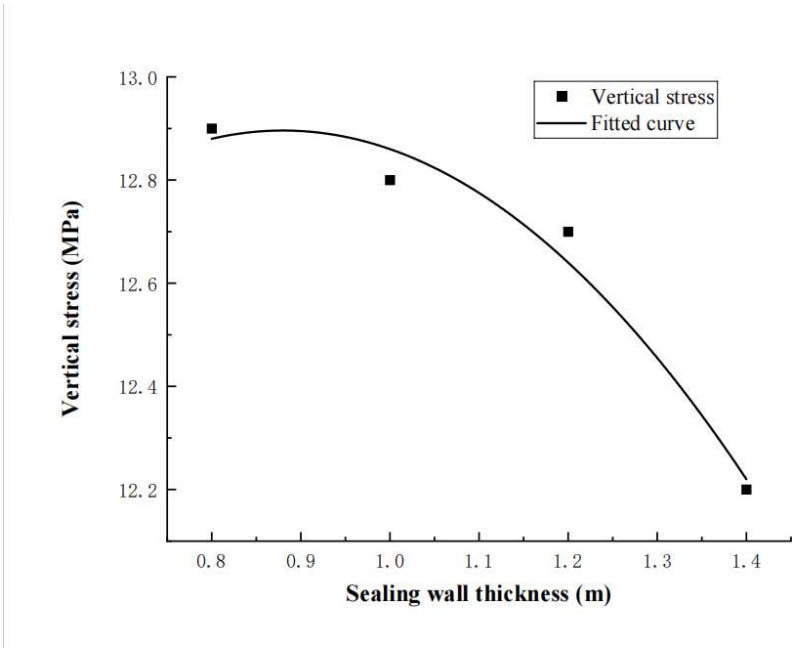


Figure 11. Relationship between the thickness of Sealing Wall B and the vertical stress.

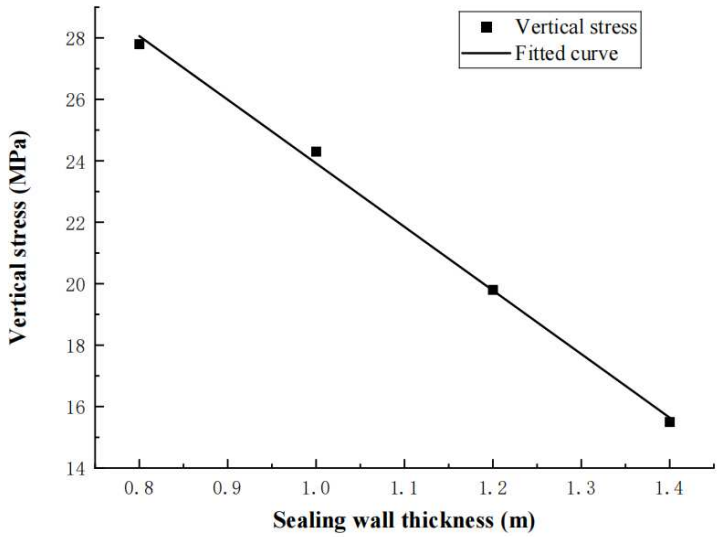


Figure 12. Relationship between the thickness of Sealing Wall C and the vertical stress.

As can be observed from the overall morphology of the two sets of fitted curves, the vertical stress sustained by the sealing wall decreases continuously with increasing thickness, exhibiting a significant non-linear negative correlation. For Sealing Wall B, as the thickness increases from 0.8m to 1.4m, the overall variation range of the vertical compressive stress is extremely narrow (the difference between its maximum and minimum values is 0.7 MPa). In contrast, Sealing Wall C shows a much larger variation range in vertical compressive stress (the difference between its maximum

and minimum values is 12.3 MPa), indicating that the stress response of Sealing Wall C is more sensitive to thickness. When the wall thickness is 0.8m, the maximum vertical stress reaches approximately 27.8 MPa; when the thickness increases to 1.0m, the maximum vertical stress drops rapidly to approximately 24.3 MPa; as the thickness further increases to 1.2m and 1.4m, the stress continues to decline to 19.8 MPa and 15.5 MPa, respectively.

Regarding Sealing Wall B (Figure 11), the vertical stress decreases relatively slowly when the thickness is small (0.8m–1.2m). However, after the thickness exceeds 1.2m, the stress shows an accelerated downward trend. Based on this non-linear characteristic, a Quadratic Polynomial model is most appropriate for fitting, expressed as:

$$y = A + B \cdot x + C \cdot x^2 \quad (3)$$

where A, B, and C are undetermined parameters related to the non-linear variation of vertical stress; y is the vertical stress (MPa); and x is the sealing wall thickness (m).

Regarding Sealing Wall C (Figure 12), the vertical stress shows a significant proportional attenuation feature as the sealing wall thickness increases. Therefore, a Linear model is adopted for fitting, expressed as:

$$y = a + b \cdot x \quad (4)$$

where a and b are undetermined parameters related to the linear variation of vertical stress.

Substituting the extracted data points into the aforementioned models, the fitted curve equations for the two groups of vertical stress are:

$$y = 10.96 - 4.40 \cdot x - 2.50 \cdot x^2 \quad (5)$$

$$y = 44.62 - 20.7 \cdot x \quad (6)$$

The fitting analysis above indicates that increasing the sealing wall thickness can effectively reduce local vertical stress concentration. The Quadratic Polynomial and Linear models accurately reflect the relationship between sealing wall thickness and vertical stress under different stress environments, providing quantitative functional expressions for the subsequent evaluation of the bearing state of the sealing wall and surrounding rock stability.

In summary, increasing the sealing wall thickness can effectively reduce the vertical stress it sustains. A 1.0m-thick sealing wall satisfies structural compressive safety requirements; considering that further increasing the wall thickness would lead to higher material and construction time costs, and combined with the conclusion from the previous displacement analysis—that a 1.0m-thick sealing wall is the critical point for rational thickness—it is comprehensively determined from the dual dimensions of safety, reliability, and techno-economic feasibility that the optimal rational thickness of the sealing wall is 1.0m.

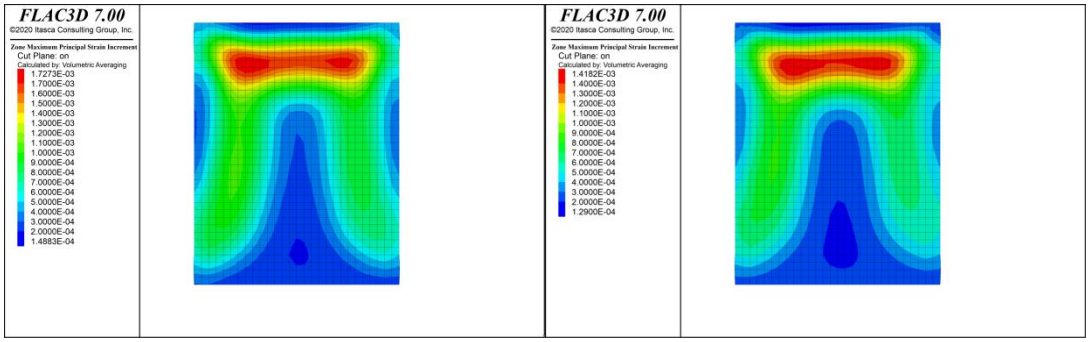
5. Study on Sealing Wall Strength

As mentioned above, under the complex coupling of shallow/deep geological environments and mining-induced stress, the thickness of the sealing wall determines the macro-scale bearing stiffness and stress distribution state of the entire sealing system. After scientifically identifying 1.0m as the optimal design thickness under these engineering conditions, the material strength of the filling body becomes the core control variable that determines whether internal failure occurs and whether the "pressure-relief and energy-absorption" characteristics of the flexible formwork can be fully utilized. Therefore, in this chapter, the thickness parameter is fixed at 1.0m to further investigate the influence of different concrete strength grades (C10–C30) on the multidimensional strain evolution characteristics of the sealing wall, aiming to achieve dual optimization of thickness and strength.

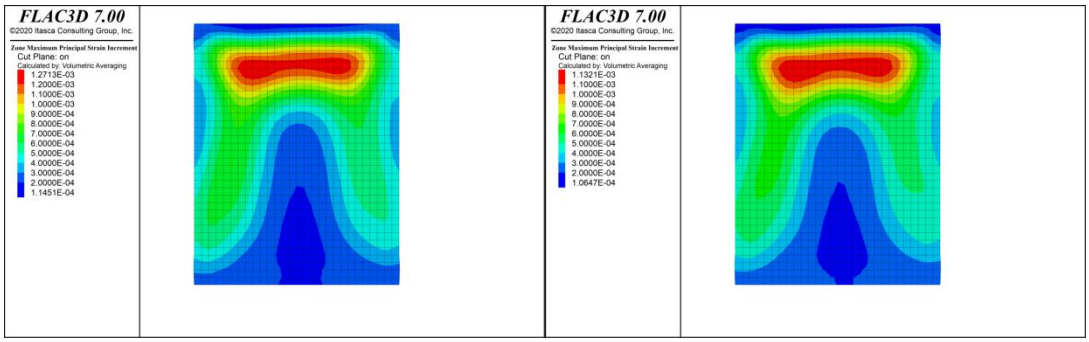
Since the measured stress within the concrete sealing wall remains essentially consistent under the same in-situ and mining-induced stresses regardless of changes in material strength, the research on sealing wall strength is conducted through deformation analysis. Given the core mechanical properties of concrete—high compressive strength, low tensile strength, and moderate shear strength—this study focuses on the maximum principal strain and maximum shear strain rather than crushing/compressive failure (i.e., the minimum principal strain). Furthermore, as determined in Chapter 4, Sealing Wall C sustains higher stress compared to Sealing Wall B. Given that both walls utilize the same concrete strength grade, Sealing Wall C experiences greater strain. Therefore, from an engineering safety perspective, this study focuses exclusively on the strain of Sealing Wall C.

5.1 Influence of Strength on the Maximum Principal Strain of the Sealing Wall

To investigate the influence of strength on the maximum principal strain of the sealing wall, the maximum principal strain cloud diagrams of Sealing Wall C under different strength grades (C10, C20, C25, and C30) were extracted for in-depth analysis, as shown in Figure 13.



（a）C10　　（b）C20



（c）C25　　（d）C30

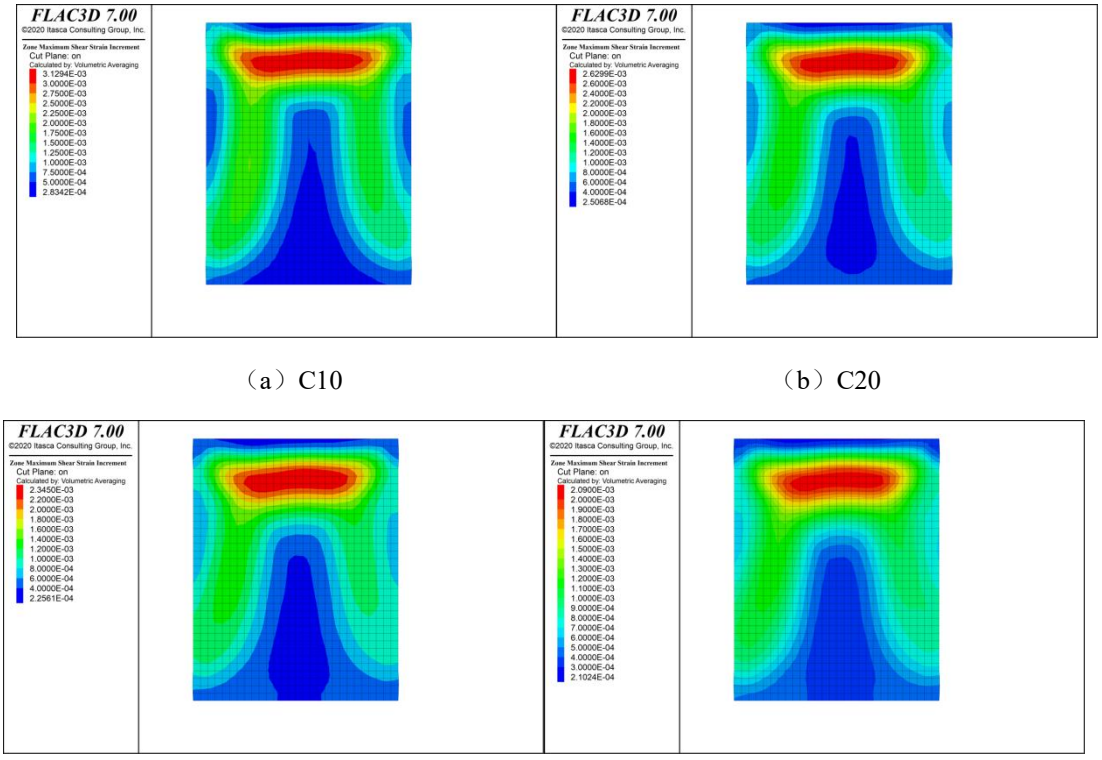
Figure 13. Cloud diagram of the maximum principal strain of Sealing Wall C.

As can be observed from the overall distribution patterns in Figure 13, compared to Sealing Wall B, the high-strain zones of Sealing Wall C exhibit a more intense "inverted U-shape" deformation characteristic (characterized by compression-induced settlement at the top and lateral squeezing-induced expansion), with a qualitative mutation in the overall strain magnitude (a sharp increase from the 10^{-4} order to the 10^{-3} order). As the concrete strength grade increases, the maximum principal strain of Sealing Wall C shows a continuous downward trend. When the sealing wall strength grade is C10 (Figure 13a), the peak maximum principal strain reaches as high as 1.73×10^{-3}. When the strength grade is increased to C20 (Figure 13b), the peak maximum principal strain drops significantly to 1.42×10^{-3}. As the strength grade is further increased to C25 (Figure 13c) and C30 (Figure 13d), the peak maximum principal strain continues to decrease steadily to 1.27×10^{-3} and 1.13×10^{-3}, respectively.

5.2 Influence of Strength on the Maximum Shear Strain of the Sealing Wall

During the loading and deformation process of the composite sealing system, the previously analyzed principal strain (tension-compression deformation) primarily reflects the volume compression and local splitting trends of the wall. In addition, shear deformation is another major cause inducing internal crack propagation and "wall-rock" interface slip failure within the sealing wall. When the maximum shear strain exceeds the material threshold, the sealing wall may develop oblique cracks, shear displacement, or even overall instability, leading directly to the failure of its fire

prevention and extinguishing functions. Therefore, to comprehensively evaluate the influence of filling body strength on the shear deformation resistance of the sealing wall, the maximum shear strain cloud diagrams of Sealing Wall C at a fixed thickness of 1.0m under different strength grades (C10, C20, C25, and C30) were extracted for comparative analysis, as shown in Figure 14.



（a）C10　　（b）C20

（c）C25　　（d）C30

Figure 14. Cloud diagram of the maximum shear strain of Sealing Wall C.

As can be observed from the overall strain distribution in Figure 14, the maximum shear strain within Sealing Wall C exhibits a highly regular "inverted U-shape" distribution pattern. As the concrete strength grade increases, the shear strain gradually decreases. When the strength grade is C10 (Figure 14a), the peak maximum shear strain surges to 3.12 × 10-3; when the strength grade is increased to C20 (Figure 14b), the peak maximum shear strain drops sharply to 2.62 × 10-3; as the strength grade is further increased to C25 (Figure 14c) and C30 (Figure 14d), the peak maximum shear strain continues to decline steadily, falling to 2.34 × 10-3 and 2.09 × 10-3, respectively.

5.3 Comparative Analysis and Determination of Rational Strength

(1) Comparative Analysis of Maximum Principal Strain

The aforementioned strain cloud diagrams qualitatively revealed the inhibitory effect of increased strength on the wall's failure morphology. To intuitively and quantitatively reveal the marginal control effect of concrete strength grade on the ultimate deformation of the sealing wall, the peak maximum principal strain values of Sealing Wall C were extracted for statistical fitting. To facilitate mathematical modeling, the concrete strength grades (C10, C20, C25, C30) were converted into continuous numerical strength variables x (x = 10, 20, 25, 30), and the relationship curve between the maximum principal strain and concrete strength was plotted, as shown in Figure 15.

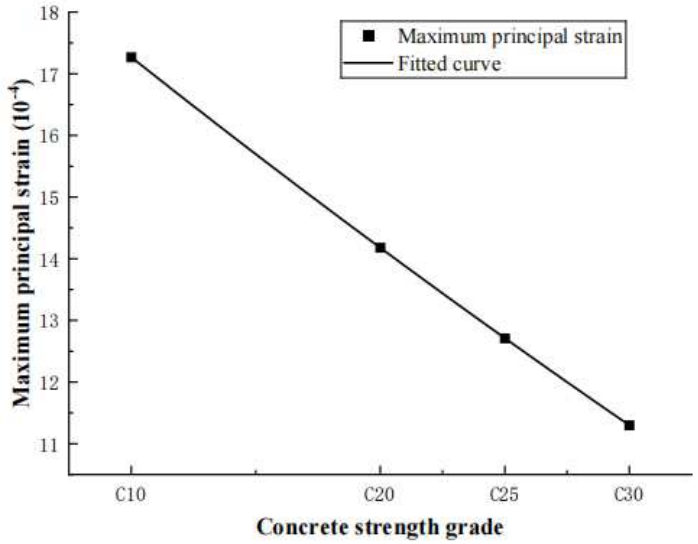


Figure 15. Relationship curve between the maximum principal strain and concrete strength grade of the sealing wall.

As shown in the figure, the maximum principal strain of seal wall C exhibits a significant linear decreasing trend with the increase in seal wall strength. This indicates that within the strength range of C10 to C30, the improvement of the concrete strength grade provides a stable and continuous benefit in controlling wall deformation, with the reduction amplitude of the principal strain remaining basically constant for every unit increase in strength.

In response to this mechanical response characteristic, adopting a linear regression model to fit and analyze the data is the most reasonable approach. The general formula for the assumed model is:

$$y = k \cdot x + b \tag{7}$$

Where k and b are undetermined parameters related to the deformation characteristics of the seal wall material, y is the maximum principal strain of the seal wall, and x is the representative value of the concrete strength of the seal wall (MPa).

By substituting the extracted coordinate values into the model for regression calculation, the fitted curve equation for the maximum principal strain of seal wall C can be obtained as follows:

$$y_C = (-3.0 \cdot x + 20.23) \times 10^{-4} \quad (8)$$

From the above fitting analysis, it is evident that the linear regression model can accurately characterize the relationship between the maximum principal strain of the seal wall and the concrete strength grade. Research demonstrates that increasing the concrete strength grade of the seal wall can effectively reduce the peak value of the maximum principal strain at a stable proportional rate, providing a solid quantitative basis for the rational material selection of the seal wall.

(2) Comparative Analysis of Maximum Shear Strain

The maximum shear strain values of Sealing Wall C under different concrete strength grades were extracted, and the concrete strength grades were converted into continuous numerical variables x (x = 10, 20, 25, 30) for quantitative analysis. The variation curve of the maximum shear strain with respect to the concrete strength grade is plotted as shown in Figure 16.

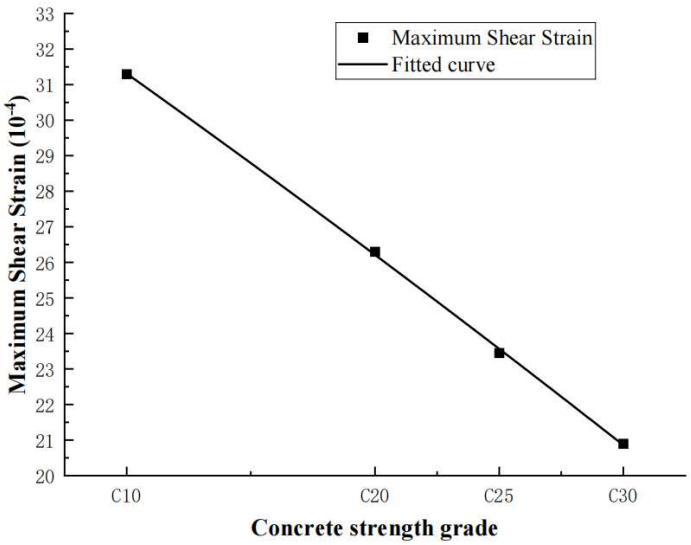


Figure 16. Relationship curve between the maximum shear strain and the strength of the sealing wall.

As illustrated in the figure, the maximum shear strain of the seal wall also demonstrates a significant linear decreasing trend as the concrete strength grade increases. Based on this mechanical response law, a linear regression model is applied to fit and analyze the maximum shear strain data. The assumed general model formula is:

$$y = (k \cdot x + b) \times 10^{-4} \quad (9)$$

Where k and b are undetermined parameters related to the shear resistance characteristics of the seal wall, y is the maximum shear strain, and x is the representative value of the seal wall concrete strength (MPa).

By substituting the extracted numerical values into the model for precise regression, the fitted curve equation for the maximum shear strain of seal wall C is determined as:

$$y_C = (-0.53 \cdot \mathrm{x} + 36.57) \times 10^{-4} \quad (10)$$

The above fitting analysis reveals that the linear model can perfectly describe the relationship between the maximum shear strain of the seal wall and the concrete strength grade. Enhancing the concrete strength grade of the seal wall can steadily decrease the peak maximum shear strain. However, in practical engineering applications for material selection, higher strength is not necessarily always better. Considering that C30 concrete has poor yielding coordination and high costs, C25 concrete can not only effectively control the maximum principal strain within the safety threshold to prevent the generation of penetrating failure cracks, but also retain sufficient flexible compression space to absorb mining-induced energy. Therefore, taking into account deformation stability, yielding characteristics, and engineering economy, the reasonable design strength grade of the seal wall is ultimately determined to be C25.

6. Mechanized Construction System and Full-Section Constraint Mechanism of Flexible Formwork Sealing Walls

Through the numerical simulation optimization conducted in Chapters 4 and 5, this study has quantitatively established the rational thickness (1.0m) and optimal strength grade (C25) for flexible formwork sealing walls in connecting roadways subjected to intensive mining-induced dynamic pressure. However, in the practical engineering construction of shallow-buried mines, traditional manual masonry or low-efficiency slurry pouring methods often lead to construction defects, such as lateral bulging of the flexible formwork bags (resulting in actual thicknesses far exceeding 1.0m and causing material waste) or inadequate roof contact (leading to local stress

concentration and air leakage). Consequently, these defects prevent the "optimal parameters" derived from theoretical design from being accurately implemented in the field. Therefore, to ensure that the 1.0m-thick C25-strength paste materials are formed with high quality and efficiency underground, this paper proposes and applies a set of rapid construction technologies for flexible formwork sealing walls based on a vehicle-mounted pumping system. By establishing a "skeleton-flexible skin" synergistic constraint mechanism, the in-situ high-pressure forming and precise control of the sealing walls are achieved.

6.1 Vehicle-Mounted Pumping Equipment and Spatial Skeleton Constraint System

The core hardware basis of the novel flexible formwork construction process lies in the highly integrated underground mobile filling pump vehicle system (see Figure 17). This system utilizes an explosion-proof diesel chassis as a carrier and highly integrates double-tank interconnected flat-opening storage cylinders, high-power plunger-type filling pumps, and pitching boom-type delivery pipelines capable of multi-degree-of-freedom adjustment. This integrated design effectively overcomes the challenge of pipeline clogging during long-distance transportation in deep underground mines, enabling continuous mixing and in-situ pumping of quick-setting high-water materials, thereby providing continuous power support for the rapid pouring of sealing walls.

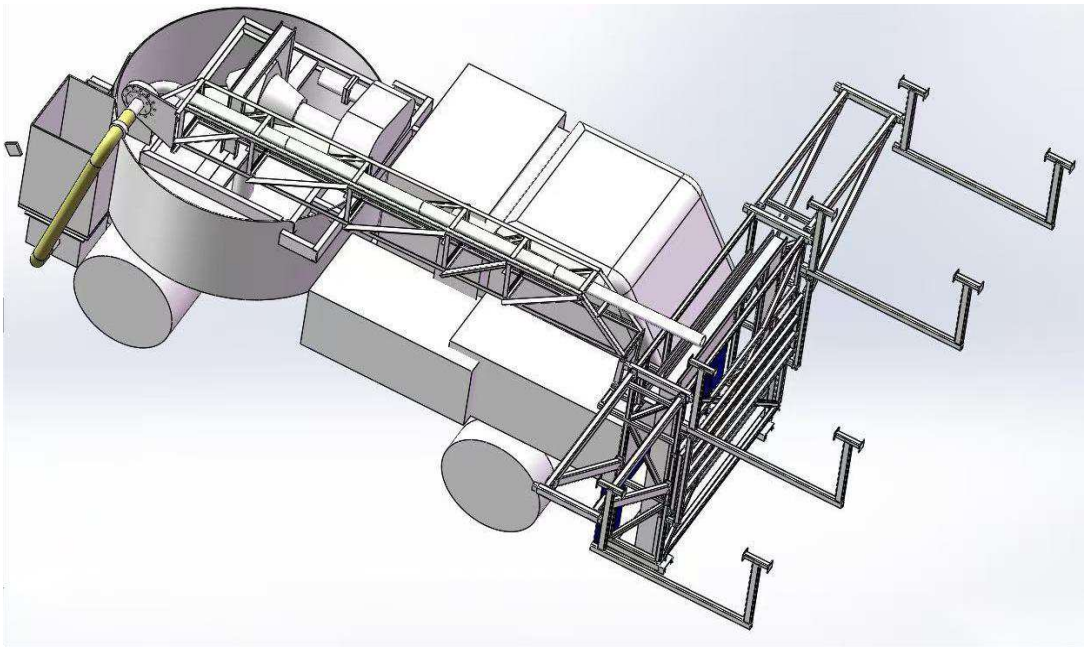


Figure 17. Schematic diagram of the integrated underground mobile vehicle-mounted pumping system.

In terms of constructing the internal spatial boundaries of the sealing wall, a flexible formwork spatial support system (see Figure 18) was designed. This system serves as

the initial spatial geometric constraint skeleton for the sealing wall, which is primarily assembled from floor-positioned transverse steel pipes, adjustable mechanical struts, sleeve structures, and interspersed cross-braces. By deploying retractable struts between the two transverse steel pipes, stable and adjustable initial anti-lateral instability stiffness is provided for the entire flexible formwork system, thereby ensuring the precise implementation of the thickness design parameter (1.0m) within the complex roadway cross-section.



Figure 18. Schematic diagram of the flexible formwork spatial supporting skeleton structure.

6.2 Configuration of High-Strength Flexible Formwork and In-Situ Precise Roof-Contact Technology

To achieve adaptive coupling between the filling paste and the significant deformation of the surrounding rock in the roadway, this process utilizes high-strength double-layer fiber fabric sewn into an integrated flexible formwork filling bag (see Figure 19). Its three-dimensional dimensions are pre-set to be slightly larger than the actual excavation cross-section of the roadway, thereby ensuring that the bag can fully expand after high-pressure pumping and fill into the deep portions of the pre-cut peripheral rock slots.

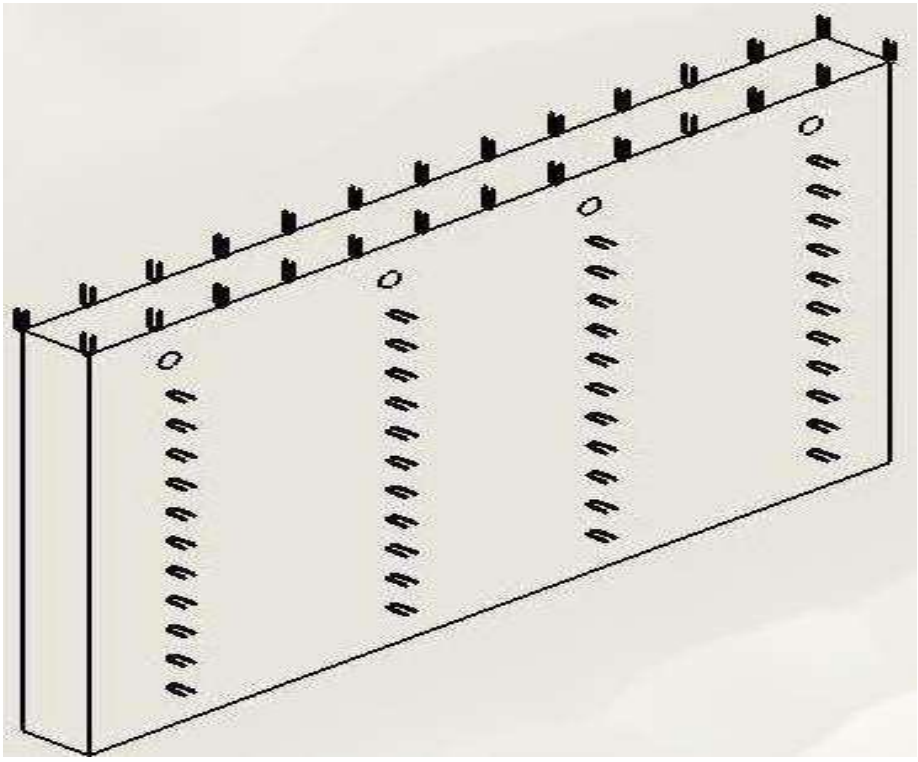


Figure 19. Schematic diagram of the structural characteristics of the high-strength fabric flexible formwork filling bag.

In large-section connecting roadways, the suspension of flexible formwork bags and full-section roof contact are the core challenges for air leakage control. This process achieves mechanized precise roof contact through a grouting nozzle coupled with a work platform at the front end of the pump truck: during the initial positioning stage, the work platform is manipulated to drive the customized concave rack to rise vertically, steadily supporting the transverse steel pipes of the flexible formwork support skeleton from bottom to top. Driven by hydraulic lifting force, the vertical struts are passively extended, pushing the entire flexible formwork filling bag steadily and forcefully to the roof elevation of the roadway. This mechanized lifting mechanism forces the upper edge of the bag to be deeply embedded into the roof slots, achieving absolute confinement of the flexible formwork system in three-dimensional space, and fundamentally eliminating the "roof contraction and void" hazard typically associated with traditional gravity pouring.

6.3 Internal Tension Anti-Deflection and Deformation Control Mechanism during the Filling Rheological Stage

During the high-pressure continuous pumping stage of the quick-setting paste material, the internal flexible formwork bag is subjected to rapidly increasing hydrostatic pressure and dynamic load impacts. To effectively suppress non-uniform bulging (i.e., the "bulging" effect) or overall lateral sliding of the 1.0m-thick wall in

its non-set state, the system introduces a multidimensional synergistic anti-lateral bulging mechanism.

Inside the flexible formwork bag, high-tensile reinforcement ropes are distributed in an orthogonal array on the inner surface, and penetrating internal tie-rods are laid along the areas corresponding to the vertical support struts. Under the lateral extrusion of the paste, these internal reinforcement bands are passively tensioned, generating a significant servo-tension effect that directly offsets the lateral fluid compressive stress. Simultaneously, a rigid scaffolding row system is temporarily installed on both the front and rear sides of the bag exterior. This fluid-structure coupling deformation control mechanism—"internal tension reinforcement + external skeleton extrusion resistance"—strongly inhibits the early lateral deformation of the wall, ensures the flatness and stress uniformity of the load-bearing cross-section of the sealing wall after pouring, and enables the design thickness parameters to be perfectly translated into actual engineering structural performance.

7. Conclusions

Addressing the engineering challenges of low construction efficiency and susceptibility to air leakage due to mining-induced dynamic pressure in sealing walls within connecting roadways of shallow-buried mines, this study has systematically investigated the influence of sealing wall thickness and strength on surrounding rock deformation and structural stability through numerical simulation. Furthermore, a rapid construction technology for flexible formwork sealing walls based on a vehicle-mounted pumping system was proposed and applied. The main conclusions are as follows:

(1) The diminishing marginal effect of sealing wall thickness on surrounding rock displacement and wall stress has been revealed. The maximum roof displacement exhibits a non-linear exponential decay characteristic as the sealing wall thickness increases, with 1.0m identified as the efficiency "inflection point" for displacement control. Within this interval, increasing the thickness from 0.8m to 1.0m reduces roof subsidence by more than 50%. Simultaneously, 1.0m is the critical boundary for the key Sealing Wall C to transition from a dangerous critical state to a safe bearing zone; the mechanical benefits of further increasing the thickness tend to diminish. Therefore, the rational design thickness is determined to be 1.0m.
(2) The control mechanism of sealing wall strength on the deformation and failure of the composite sealing system has been clarified. Sealing Wall C, which is subjected to intense asymmetric mining-induced abutment pressure, serves as the control zone for the entire system. Low-strength (C10) materials lack sufficient resistance to deformation, posing significant risks of penetrating shear tearing and air leakage. Conversely, excessively high-strength (C30) materials render the

structure overly rigid, causing it to lose the pressure-relief and energy-absorption characteristics inherent to the flexible formwork system.

(3) A non-linear "strength-strain" synergistic control model for the sealing wall has been established. Through statistical fitting of the maximum principal strain and maximum shear strain data, a response equation centered on exponential decay was developed. The C25 strength grade serves as the optimal strength grade within the "rigid-flexible synergistic equilibrium zone," effectively balancing the contradiction between deformation control and pressure relief. Consequently, the optimal design parameter combination for the flexible formwork sealing wall in connecting roadways under intensive mining is determined as a rational thickness of 1.0m and a rational strength grade of C25.

(4) A set of mechanized construction technologies for flexible formwork sealing walls based on a vehicle-mounted pumping system has been proposed and improved. By utilizing an integrated underground mobile filling pump vehicle, combined with a "spatial skeleton constraint system" and high-strength fabric flexible formwork bags, full-section precise roof contact and in-situ high-pressure forming of the sealing wall are achieved. This effectively solves the bottleneck issues of traditional construction methods, such as inadequate roof contact and susceptibility to cracking and air leakage under large-scale deformation.

Data Availability

The datasets used and analyzed during the current study are available from the corresponding author on reasonable request.

Conflicts of Interest

The authors declare that they have no known competing financial interests or personal relationships that could have appeared to influence the work reported in this paper.

Funding Statement

This paper is supported by the following fund project: Science and Technology Innovation Project of National Energy Investment Group Co., Ltd. (No.: GJNY-23-31-1).

References

Cao, X., S. Wang, X. Wang, et al., 2025, "Research analytics on the applications of flexible formwork gob-side entry retention technology in medium-thickness coal seams with large inclination angles," PloS one, 20, no. 5, e0323337.

Chen, Z., 1966, "My views on the article 'Rational calculation of waterproof sealing walls'," Journal of China Coal Society, no. 01, 61-71.

Cheng, J., and X. Zhang, 2021, "Damage assessment of mine seal under blast impact load," China Safety Science Journal, 31, no. 01, 132-137.

Douglas, A., 2006, "History of the development and deployment of the parallel sided mortar intrusion concrete watertight bulkhead in underground mines," Journal of the Southern African Institute of Mining and Metallurgy, 106, no. 5, 311-316.

Du, M., F. Kong, and Y. Fei, 2025, "Stability evaluation and position optimization of waterproof sealing walls in connecting alleys," Advanced Engineering Sciences, 57, no. 01, 264-273.

Guo, R., J. Martino, and D. Dixon, 2005, "Fully coupled thermohydraulic modelling of the sealing bulkheads and adjacent rock in a full-scale underground test," Canadian Geotechnical Journal, 42, no. 5, 1318-1329.

Harteis, S., and D. Dolina, 2006, "Water and slurry bulkheads in underground coal mines: design, monitoring and safety concerns," Mining Engineering, 58, no. 12, 41-47.

Hu, H., B. Zhang, X. Zhang, et al., 2025, "Numerical simulation of gas explosion law and determination of safe thickness of blocking wall after auxiliary tunnel blocking," Scientific Reports, 15, no. 1, 8593-8593.

Huang, J., D. Qiao, H. Sun, et al., 2014, "Calculation and Optimizing Analysis of the Force of Filling Airtight-wall for Underground Mined-out Area," Metal Mine, no. 10, 32-36.

Jianwei, C., S. Wanting, J. Yi, et al., 2020, "Research on mine seal stability under explosion load and ground pressure in underground coal mines," Archives of Mining Sciences, 65, no. 1, 71-87.

Jing, Y., X. Zhang, and J. Cheng, 2017, "Safety Analysis of Anti-explosive and Anti-impacted Airtight Wall Based on ANSYS Numerical Simulation," Safety in Coal Mines, 48, no. 11, 194-197.

Li, D., K. Zhang, H. Yu, et al., 2008, "Research on the Mine Shock Air-bump and Ant i shock Bulkhead," Journal of Shandong University of Science and Technology (Natural Science Edition), no. 02, 14-18.

Li, H., 2015, "Numerical Simulation Stady on Characteristic Parameters of Airtight Filling with Solidification of Fiy Ash," Xi'an University of Science and Technology. (in Chinese)

Li, J., J. Kang, and S. Wei, 2020, "Deformation and Failure Characteristics of Sealing Wall Affected by Mining in Coal Pillar Face and Reinforcement Measures," Coal Technology, 39, no. 01, 13-18. (in Chinese)

Liu, F., 2019, "Numerical Simulation and Experimental Analysis of Anti-explosion Impact Pressure of Closed Wall in Coal Mine," Safety in Coal Mines, 50, no. 10, 18-21. (in Chinese)

Lu, H., T. He, and Z. Zhang, 2014, "Definition of Reasonable Parameters of Airtight Wall in Crossheading of Fully Mechanized Caving Face," Coal Technology, 33, no. 10, 118-119.

Mu, Z., 2007, "Application of mine pressure in coal mine goaf sealing walls," Tongmei Technology, no. 01, 24-25.

Sun, W., 2021, "Discussion on design method of anti-shock air stopping wall in large area overhanging roof goaf," China Mining Magazine, 30, no. S1, 301-304. (in Chinese)

Wang, H., and J. Guo, 2025, "Research on the deformation and failure mechanism of flexible formwork walls in gob-side-entry retaining of ultra-long isolated mining faces and pressure relief-control technology," Applied Sciences, 15, no. 11, 5833.

Wei, D., 2009, "Stability Analysis for New Mine Air Stopping of Goaf," Coal Technology, 28, no. 01, 10-12.

Xie, S., H. Pan, D. Chen, et al., 2020, "Stability analysis of integral load-bearing structure of surrounding rock of gob-side entry retention with flexible concrete formwork," Tunnelling and Underground Space Technology, 103.

Yan, G., 1965, "Rational calculation of waterproof sealing walls," Journal of China Coal Society, no. 03, 83-86.

Yang, Z., 2015, "Safety Assessment of Waterproof Sealing Wall Chamber with Water Storage and Utilization in Underground Goaf," Coal Mine Safety, 46, no. 10, 203-206.

Yi, L., 1976, "On the rational calculation of waterproof sealing walls," Coal Science and Technology, no. Z2, 96-99.

Yuan, H., S. Wanghua, and Y. Shichong, 2022, "Experimental investigation of the seepage failure between bulkheads and surrounding rocks in deep underground mines," Bulletin of Engineering Geology and the Environment, 81, no. 9.

Zhang, G., 2015, "Reliability study on Waterproof Air Barrage of Wulanulun Coal Mine," Coal Engineering, 47, no. 06, 67-69+72.

Zhang, J., 2021, "Numerical simulation of stess state and stability of closed seal under explosion load," China Mining Magazine, 30, no. 11, 121-128.

Zheng, X., 2002, "Design of underground sealing walls for large-scale goafs," Metal Mine, no. 12, 56-57.